ROYAL SOCIETY OF CHEMISTRY

EDGE ARTICLE

Check for updates

Delocalization tunable by ligand substitution in [L₂Al]ⁿ⁻ complexes highlights a mechanism for strong electronic coupling†

Amela Arnold, [ID] Tobias J. Sherbow, Amanda M. Bohanon, Richard I. Sayler, R. David Britt, [ID] Allison M. Smith, James C. Fettinger [ID] and Louise A. Berben [ID]*

Ligand-based mixed valent (MV) complexes of Al(III) incorporating electron donating (ED) and electron withdrawing (EW) substituents on bis(imino)pyridine ligands (I₂P) have been prepared. The MV states containing EW groups are both assigned as Class II/III, and those with ED functional groups are Class III and Class II/III in the $(I_2P^-)(I_2P^{2-})Al$ and $[(I_2P^{2-})(I_2P^{3-})Al]^{2-}$ charge states, respectively. No abrupt changes in delocalization are observed with ED and EW groups and from this we infer that ligand and metal valence p-orbitals are well-matched in energy and the absence of LMCT and MLCT bands supports the delocalized electronic structures. The MV ligand charge states $(I_2P^-)(I_2P^{2-})Al$ and $[(I_2P^{2-})(I_2P^{3-})Al]^{2-}$ show intervalence charge transfer (IVCT) transitions in the regions 6850–7740 and 7410–9780 cm^{-1}, respectively. Alkali metal cations in solution had no effect on the IVCT bands of $[(I_2P^{2-})(I_2P^{3-})Al]^{2-}$ complexes containing −PhNMe₂ or −PhF₅ substituents. Minor localization of charge in $[(I_2P^{2-})(I_2P^{3-})Al]^{2-}$ was observed when −PhOMe substituents are included.

Introduction

Studies on the classic transition metal MV system, the Creutz–Taube (C–T) ion: $[\{(NH_3)_5Ru\}_2pz]^{5+}$, have shown that delocalization of the unpaired electron can be tuned extensively *via* variations in metal identity, ancillary ligands, and the identity of the bridging pz ligand (Chart 1A).[1–4] As examples, when NH₃ ligands are replaced with bpy,[5] or CN ligands,[6] the EW nature of those ligands affords a decrease in the electronic coupling between the two Ru ions from Class III to Class II. Competition for the metal π-symmetry d-electrons from the π-acceptor ancillary ligands and the bridging pyrazine is thought to diminish delocalization of the electron between Ru atoms. No abrupt changes in delocalization/localization occur as a result of changes to the nature of ligand–metal bonding between, for example, π-accepting *vs.* π-donating ligands.

MV organic molecules are harder to study because synthesis of analogs is often challenging. The MV state of an organic molecule is often a reactive radical cation or anion with dimerization or disproportionation pathways available for decomposition.[7,8] For example, triarylamine compounds are only synthesized with R = OMe protecting groups in the *para*

position to avoid coupling of the two cationic radicals tail to tail,[7,9] and dithiafulvenyl compounds undergo dimerization of the MV radical cations when substituted with EW groups.[10,11]

Disproportionation of the MV state has been observed for MV naphthidines with ED groups, whereas EW groups, such as fluorine favored formation of the oxidized dications.[12] Although limited by synthetic challenges in many instances, the effect of ED or EW substitution on organic MV systems including phenylenediamine,[13] bis(triarylamine),[14] or naphthidine radical cations,[12] has been explored: in all cases the MV states are strongly coupled "charge resonance" compounds and the coupling is not significantly affected by substitution of ED and EW substituents on the end-groups.[13,15] The compounds are all considered Class III delocalized. Aryl hydrazine radical cations offer a rare exception, where electronic coupling is greatest when R = OMe, *vs.* R = Br, Cl, I, CN or NO₂ where coupling is reduced to Class II/III (Chart 1B).[16]

Department of Chemistry, University of California, 1 Shields Ave., Davis, CA, 95616, USA. E-mail: laberben@ucdavis.edu
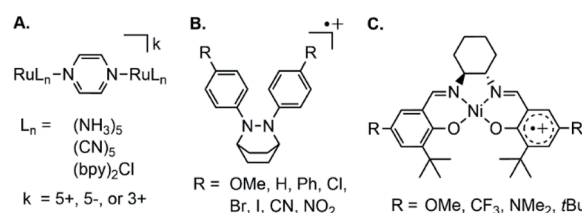
Chart 1 Example mixed valent (MV) complexes where electron donating and electron withdrawing functional groups have been varied to understand delocalization.
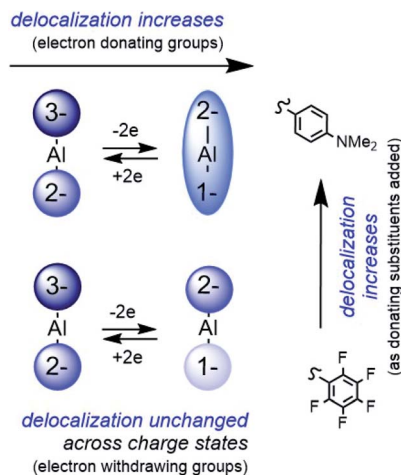
Chart 2 Electron delocalization is predictably tuneable *via* ED and EW groups. This is possible because IVCT transitions are not convoluted with LMCT and MLCT transitions. Valence p-orbitals on metal and ligands dictate available transitions.

Another class of metal-containing MV compound are those in which a metal center bridges two redox-active organic end groups, and in those complexes the organic group is referred to as a redox-active ligand.[17] Here again, well-characterized and predictably tunable electronic coupling has not been achieved by substitution of EW and ED groups on the organic end groups. The majority of ligand-based MV complexes are bridged by transition metals and the unpaired electron associated with those MV end-groups is most often localized.[18–20] Square planar complexes of d^8 metals Ni(II), Pd(II), Pt(II) as well as Au(III) are delocalized,[21] with some exceptions.[22] Those systems can be hard to fully understand because ambiguity in the assignment of metal and ligand charge states, along with convolution of LMCT bands with IVCT bands is common. In addition, as ED and EW groups are added, changes to the nature of the ligand–metal interaction result: variation between π-donating to π-accepting character can result from ED and EW group substitution and cause unpredictable changes to electronic coupling. This situation was encountered with a series of Ni salen metal complexes (Chart 1C):[18,23–25] EW substituents impart delocalization, and ED substituents impart localization. Those effects were rationalized by considering that ED groups enable greater donation by the ligand into empty Ni(II) d-orbitals and then orbital pathways for delocalization through the ligand are not available.

We have recently been studying ligand-based MV compounds with Group 13 metals as the bridging ion.[26] Our initial studies provided experimental evidence that bis(imino) pyridine (I₂P) redox-active ligands bridged by Group 13 metals display Class III behavior and are delocalized. We also noted in that work that the octahedral coordination geometry enables ligand donor atoms to achieve good orbital overlap with metal p-valence orbitals, and we reasoned that this may facilitate the strong coupling between the two ligand end-groups. That work did not provide any insights as to why Class III, delocalized was observed with the Group 13 central ion.

In the present report we have used a systematic synthetic chemistry approach to understand the origin of the delocalized MV states observed in Al-bridged redox-active ligand complexes. Substituents on the I₂P ligands were varied between ED and EW and we observed no abrupt changes in the extent of delocalization as a result of the changes in ED or EW substituents (Chart 2). This contrasts with results observed in transition element systems where ED and EW substituents on organic end groups can have unpredictable effects on delocalization or localization as the nature of metal–ligand interactions change. We can further infer from these results that the delocalized electronic structure of '(I₂P)₂Al' complexes arises because there are no available orbital pathways to support LMCT or MLCT transitions that compete with the IVCT transitions. The synthetic tunability of these compounds is reminiscent of transition element MV systems, while the strong electronic coupling, unperturbed by LMCT and MLCT transitions common to transition element systems, is more reminiscent of organic MV compounds. If it is true that the delocalized structure of '(I₂P)₂Al' is enabled by the absence of LMCT and MLCT transitions, then there is immense scope for the design of new, delocalized MV materials that incorporate main group elements with redox-active ligands, as long as orbital pathways for delocalization are incorporated.

Results and discussion

Synthesis of compounds

To access MV redox-active ligand Al complexes in which EW and ED groups are included in the organic framework we targeted two new I₂P ligands in which the aryl substituents are the ED group –PhNMe₂ ($_{NMe2}$I₂P) or the EW group –PhF₂ ($_{F5}$I₂P). Our prior report on MV I₂P complexes included –PhOMe substituents ($_{OMe}$I₂P). The syntheses of those new ligands are described in the ESI† and each I₂P ligand was characterized by ^{1}H, ^{19}F ($_{F5}$I₂P only) and ^{13}C NMR (Fig. S1–S5†), high resolution mass spectroscopy (HRMS), and UV-Vis-NIR spectroscopy. In the present study, we synthesized and fully characterized the MV members of the ligand-based charge series where the I₂P ligands have −1 and −2 charges, as in previously reported ($_{OMe}$I₂P⁻)($_{OMe}$I₂P²⁻)Al (**1**). To enable study of the MV complexes where ligands have −2 and −3 charge we generated those *in situ* as is described later in the discussion of NIR spectroscopic properties.

The synthesis of MV ($_{F5}$I₂P⁻)($_{F5}$I₂P²⁻)Al (**2**) was performed in one step: two equivalents of $_{F5}$I₂P were stirred with one equivalent of AlCl₃ for 10 minutes. Three equivalents of Na were then added to the solution and this was stirred for three days at room temperature during which time the solution gradually became darker, until it was red-brown. Isolation of **2** was achieved in 52% yield, and the compound has $\mu_{eff} = 2.06\ \mu_B$, consistent with one unpaired electron on the complex (Scheme 1). MV ($_{NMe2}$I₂P⁻)($_{NMe2}$I₂P²⁻)Al (**3**) was synthesized similarly to the approach used to obtain **1**. Reduction of $_{NMe2}$I₂P with three equivalents of Na overnight, was followed by dropwise addition of one equivalent of AlCl₃ in THF. Brown-red **3** was isolated in 15% yield and has $\mu_{eff} = 1.60\ \mu_B$. The stability of **3** even under a nitrogen
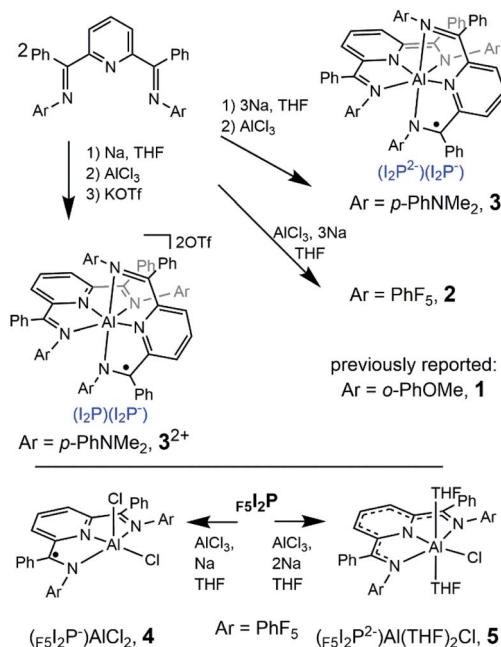
Scheme 1 Synthesis of MV Al(III) complexes **2**, **3**, **3**$^{2+}$, **4**, and **5**. Compound **1** was previously reported.[26]

atmosphere is poor, and isolation in high yield has not been possible. Each of **2** and **3** were characterized using HRMS, combustion analysis, and UV-Vis-NIR spectroscopy. In the UV-Vis region of the optical spectra of **2** and **3** the ligand-based electronic transitions were observed at 351 and 409 nm, respectively. These have extinction coefficients 22 400 and 29 600 L mol^{-1} cm^{-1} in **2** and **3**, respectively (Fig. S8†), as compared with those in the free ligand which are 2840 and 7300 L mol^{-1} cm^{-1}, respectively. These observations are consistent with previous work on Al(III) complexes with bidentate iminopyridine ligands (IP),[27] and with work on cobalt complexes with redox-active terpyridine (tpy) ligands.[28] The comparisons suggest that the transitions observed in the UV-Vis region of the spectrum can be assigned to ligand-based π–π* transitions.

MV [[(NMe$_2$I$_2$P$^-$)(NMe$_2$I$_2$P)Al](OTf)$_2$ (**3**$^{2+}$), was obtained by following a similar procedure as the synthesis of **3** but employing just one equivalent of Na. Addition of 1.1 equivalents of KOTf to the reaction mixture followed by workup enabled isolation of **3**$^{2+}$ in 33% yield, and **3**$^{2+}$ has μ_{eff} = 1.73 μ_B. The isolation of **3**$^{2+}$ was more facile than **3**, and so it was used to generate other charge states of the **3** series in subsequent studies of optical electron transfer (*vide infra*). Full details on the syntheses of all new compounds reported here can be found in the ESI.†

Complexes containing a single ligand were also synthesized and analyzed: we need to understand these in order to correctly assign which spectral features arise from the MV properties of **1**–**3** and of **1**$^{2-}$–**3**$^{2-}$. Synthesis of ($_{F5}$I$_2$P$^-$)AlCl$_2$ (**4**) and of ($_{F5}$I$_2$P^{2-})AlCl(THF)$_2$ (**5**) were performed by mixing $_{F5}$I$_2$P, AlCl$_3$ and one or two equivalents, respectively, of Na metal. After three days, and following workup, **4** and **5** were obtained in 70 and 87% yield,

respectively (Scheme 1). Both compounds were characterized by elemental analysis and X-ray crystallography. Paramagnetic **4** has μ_{eff} = 1.40 μ_B, and diamagnetic **5** was characterized by ^{1}H, ^{13}C and ^{19}F NMR spectroscopy (Fig. S6 and S7†). The UV-Vis spectra of **3**$^{2+}$ and **4** agree well with previously reported **1**$^{2+}$ and ($_{OMe}$I$_2$P$^-$)AlCl$_2$ (Fig. S8†). We were unable to synthesize the analogous mono-ligand complexes using $_{NMe2}$I$_2$P.

Solid-state structures

The solid-state structures of **2**–**5** were probed using single crystal X-ray diffraction data collected at 77 K. All experimental methods of crystal growth, data collection and refinement, and tables of bond lengths and angles are included in the ESI (Tables S1, S2 and Chart S1†). The charge state of each ligand in the complexes can be definitively assigned using the bond lengths determined crystallographically. As an example, elongation of the C–N$_{im}$ bond is expected as the ligand is reduced: 1.32–1.34 Å is typical for one-electron reduction of the imino group, and 1.41–1.45 Å for two-electron reduction of the imino group to a C–N$_{am}$ single bond (Chart 3). Reduction is most often localized at the imino carbon, but delocalization of the added electrons throughout the ligand framework is also observed in some cases and this results in intermediate bond lengths between those reported for single or double reduction.

Both **2** and **3** have one ligand of −1 and one ligand of −2 charge (Fig. 1, 2 and Tables S1, S2†). Those two tridentate ligands are arranged in a pseudo-octahedral geometry (Fig. 1). Complex **3** sits on a crystallographic symmetry element in the unit cell and so half of the structure is generated by symmetry and a detailed comparison to **1** and **2** is not possible. In **2** the radical of the −1 ligand is localized on one imino functional group, as determined from the C–N bond lengths which are 1.298(5) and 1.355(4) Å (Table S2†). The C–N bond distances also fall over a broader range than in **1**: 1.424(4) and 1.317(5) Å. The asymmetry of the I$_2$P^{2-} ligand is also reflected in the M–N bond lengths: 1.950(3) and 2.155(3) Å. For each of the MV complexes, histograms of C–N bond distance illustrate distribution of the charge between the two ligands and within each ligand, in the solid-state structures (Fig. 2). **2** has the most asymmetry and the differences between the longest and shortest C–N bond distances are the greatest. The C–N bond distances in **1** are nearly all equivalent and the average geometrical parameters for **3** lie between those of **1** and **2**.

The complexes containing a single monoanionic ligand, **3**$^{2+}$ and **4**, exhibit similar electronic structure as reported for ($_{OMe}$-I$_2$P$^-$)AlCl$_2$ (Tables S1, S2 and Fig. S9†). The radical is delocalized over I$_2$P in both cases, with C–N bond distances on the I$_2$P$^-$

Chart 3 C–N and M–N bond length designations used throughout the text. im = imine, am = amine.

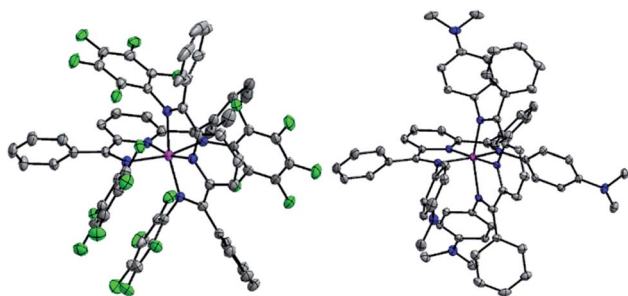|	
1	d(C-N$_{imine}$ or C-N$_{im}$)
2	d(C-N$_{amine}$ or C-N$_{am}$)
3	d(M-N$_{amine}$ or M-N$_{am}$)
4	d(M-N$_{imine}$ or M-N$_{im}$)

Fig. 1 Solid state structures of in **2** (left) and **3** (right). Light green, blue, pink and gray ellipsoids represent F, N, Al and C atoms, respectively. Ellipsoids are shown at 30% probability level. Solvent molecules and hydrogen atoms have been omitted for clarity.

ligand falling within a narrow range: 1.321(2) and 1.330(3) Å, for **4**. Mirror symmetry for **5** also appears with C–N bond lengths 1.378(4) and 1.377(5) Å, and M–N_{im} bond lengths that are nearly equivalent: 2.012(3) and 2.008(3) Å.

Electrochemical measurements

Cyclic voltammograms (CV's) of **2** and **3** were taken in 0.1 M nBu$_4$NBF$_4$·MeCN solution and display five ligand-based redox events spanning 2.19 and 1.85 V, respectively (Fig. 2 and Table 1). As previously described for **1**, these include charge states spanning $[(I_2P)(I_2P^-)Al]^{2+}$ ($\mathbf{A^{2+}}$) up to $[(I_2P^{3-})(I_2P^{3-})Al]^{3-}$ ($\mathbf{A^{3-}}$).
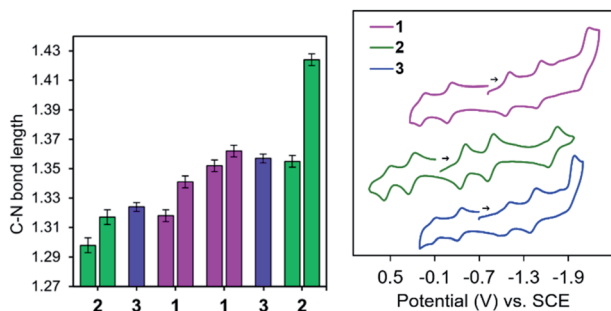

Fig. 2 (left) Histogram depicting the shortest (left) and longest (right) C–N bond lengths (Å, esd is error bars), for mixed valent **1** (pink), **2** (green) and **3** (blue/purple). (right) CV's of 0.1 mM **1** (pink), **2** (green) and **3** (blue) in 0.1 M nBu$_4$NBF$_4$·MeCN.
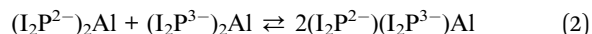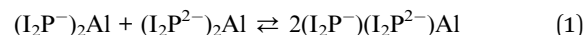
Table 1 Formal potentials ($E_{1/2}$), and peak-to-peak potentials (ΔE_p), for **2** and **3** obtained from CVs in 0.1 M nBu$_4$NBF$_4$·MeCN (**1** is included for comparison). **A** = each complex

	$E_{1/2}$ (V vs. SCE)			ΔE_p		
	1	**2**	**3**	**1**	**2**	**3**
$\mathbf{A^{2+/1+}}$	0.06	0.53	−0.08	72	82	79
$\mathbf{A^{1+/0}}$	−0.30	0.20	−0.44	72	86	71
$\mathbf{A^{0/1-}}$	−1.08	−0.49	−1.09	58	75	88
$\mathbf{A^{1-/2-}}$	−1.51	−0.87	−1.46	72	93	93
$\mathbf{A^{2-/3-}}$	−2.12	−1.66	−1.93	125	56	86
$\Delta\Delta E_{1/2}$	2.18	2.19	1.85			

The final redox event, corresponding to the $\mathbf{A^{2-/3-}}$ couple, is irreversible for **1** and **3**, at $E_p = -2.12$ V and −1.93 V vs. SCE and reversible for **2**, at $E_{\frac{1}{2}} = -1.66$ V vs. SCE. There is an expected anodic shift in redox events upon changing the ligand from ED **1** or **3** to EW **2**; for example the $E_{1/2}$ for the $\mathbf{A^{0/1-}}$ redox couple is at 0.06 V vs. SCE for **1** and shifted by −140 and +470 mV for **3** and **2**, respectively.[29,30] At very negative potentials **2** and **3** show signs of decomposition over time.

For **1** and **2**, we performed variable scan rate experiments to ensure redox events are reversible; plots of current versus sqrt of scan rate were linear for the first four couples (Fig. S10 and eqn (S1)†). To further probe for ion-pairing or coulombic/electrostatic effects, CV's for **2** and **3** were also recorded in THF ($\varepsilon = 7.58$), for comparison to the data collected in MeCN ($\varepsilon = 36.6$): minor variations were observed and are highlighted in the ESI (Table S3†).[31]

The determination of comproportionation equilibrium constants (K_c) was performed to compare **1–3** (Table 2), and these are calculated using the separation between successive redox couples, $\Delta E_{1/2}$ (eqn (S2)†). The comproportionation reaction for the MV charge states discussed here, $(I_2P^-)(I_2P^{2-})Al$ (**A**) and $(I_2P^{2-})(I_2P^{3-})Al$ (**A^{2-}**), are given by eqn (1) and (2), respectively:

$$(I_2P^-)_2Al + (I_2P^{2-})_2Al \rightleftarrows 2(I_2P^-)(I_2P^{2-})Al \quad (1)$$

$$(I_2P^{2-})_2Al + (I_2P^{3-})_2Al \rightleftarrows 2(I_2P^{2-})(I_2P^{3-})Al \quad (2)$$

The measured K_c values for **2** and **3** were on the order of 10^{11} and 10^{10}, respectively (Table 2). For comparison, **1** has measured K_c value of 10^{13}. In general, values exceeding $K_c = 10^{7.3}$ in acetonitrile suggest a delocalized electronic structure.[32] The solvent independence between CV's collected in THF and MeCN further suggests that electrostatic effects are not playing a large role in the observed electrochemical behavior and that we can attribute the spacing between successive redox events to a delocalized electronic structure for **2** and **3** (Table S4†), as we reported for **1**.[33] In general, K_c values determined using electrochemical methods are greatly over-estimated and so the numbers discussed above provide only a guideline and provide support for the conclusions drawn from the spectroscopic studies that are discussed below.[34]

NIR absorption spectra

To quantify the degree of electronic coupling between redox active ligands in MV **2**, K_2-**2**, **3**, and K_2-**3**, their absorption spectra in the near infra-red (NIR) range of the electromagnetic spectrum were collected and analysed (Fig. 3 and Table 3). In each of the spectra collected between 526–2500 nm (19 000–4000 cm^{-1}), we observed a broad band with ν_{max} between 6900 and 9780 cm^{-1} which is assigned as the inter-valence charge transfer (IVCT) transition (vide infra). We also observed a sharper, lower energy band with ν_{max} between 5200 and 5300 cm^{-1} and which appears as a low energy shoulder on the IVCT band. We assigned the lower energy feature to a ligand-based $\pi^*-\pi^*$ transition associated with the ligands having −1

Table 2 K_c values and $\Delta E_{1/2}$ values for A^+, A, A^- and A^{2-} obtained from CV data collected in 0.1 M Bu$_4$NPF$_6$·MeCN. A is any of **1–3**

		1	**2**	**3**
$(I_2P^-)_2M$	**A$^+$**	1.3×10^6 (0.36 V)	4.0×10^5 (0.33 V)	1.1×10^6 (0.36 V)
$(I_2P^-)(I_2P^{2-})M$	**A**	1.8×10^{13} (0.78 V)	4.8×10^{11} (0.69 V)	9.7×10^{10} (0.65 V)
$(I_2P^{2-})_2M$	**A$^-$**	1.6×10^7 (0.43 V)	2.7×10^6 (0.38 V)	1.8×10^6 (0.37 V)
$(I_2P^{2-})(I_2P^{3-})M$	**A^{2-a}**		2.4×10^{13} (0.79 V)	

^{a} The K_c values and $\Delta E_{1/2}$ values are not given for **1^{2-}** and **3^{2-}** because the $E_{1/2}$ (**A$^{2-/3-}$**) couples are not reversible.
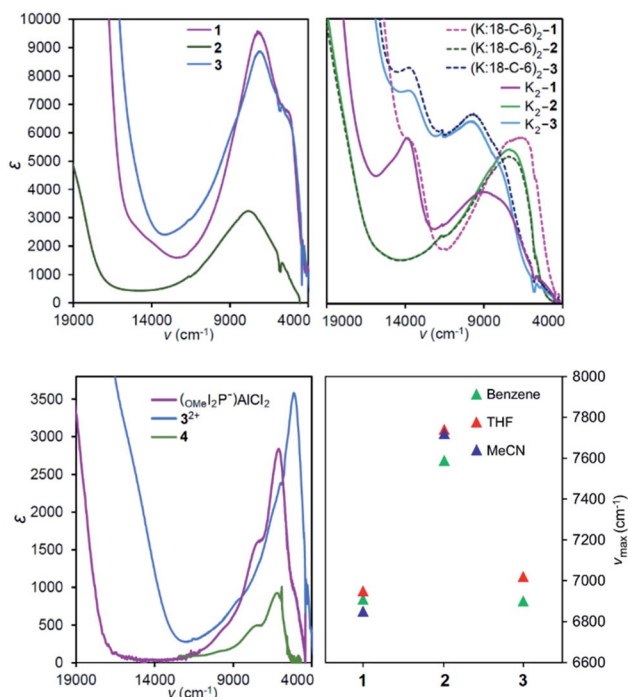

Fig. 3 NIR spectra in THF of (top left) **1**, **2** and **3**; (top right) **1^{2-}**, **2^{2-}** and **3^{2-}** *in situ* generated with potassium metal reductant, solid lines; and when 18-C-6 was added to sequester the potassium counteraction, dashed lines; (bottom left) **3^{2+}**, **4**, and ($_{OMe}$I$_2$P$^-$)AlCl$_2$, and (bottom right) ν_{max} of NIR absorption bands of **1**, **2**, and **3** in solvents spanning dielectric constant range of 34: benzene ($\varepsilon = 2.28$), THF ($\varepsilon = 1.89$), and MeCN ($\varepsilon = 36.6$).

charge state, in accordance with several prior reports of organic anion radicals where $\pi^*-\pi^*$ transitions occur at similarly low energy.[27,35–37]

An alternative model which we considered but do not favor for assignment of the NIR spectra, is a three-state model where the lower energy band would be ligand–metal charge transfer (LMCT), and the higher energy band is the IVCT.[38,39] However, complexes containing a single ligand with -1 charge: **4** and ($_{OMe}$I$_2$P$^-$)AlCl$_2$, display overtones at higher energy and this supports their assignment as ligand-based $\pi^*-\pi^*$ transitions (Fig. 3 bottom left, S11†). In addition, the energies for the low-energy transition in **4** and ($_{OMe}$I$_2$P$^-$)AlCl$_2$ are nearly identical and this is not consistent with a LMCT band assignment since the ligand frontier orbitals should have different energies in each compound (Fig. 3 bottom left). The remainder of the discussion surrounding NIR spectra assumes the low energy bands between 5200 and 5300 cm^{-1} are $\pi^*-\pi^*$ transitions.

In THF solution, the $\pi^*-\pi^*$ transition was observed at 5200 and 5300 cm^{-1} for **1** and **3**, respectively, and was not observed for **2** (Fig. 3). Comparison with the spectra of mono-ligand complexes, ($_{OMe}$I$_2$P$^-$)AlCl$_2$ and **4** indicates that in **4** the $\pi^*-\pi^*$ transition is much lower in intensity than was observed for ($_{OMe}$I$_2$P$^-$)AlCl$_2$: $\varepsilon = 780$ for **4** compared with 2320 L mol^{-1} cm^{-1} for ($_{OMe}$I$_2$P$^-$)AlCl$_2$ (Fig. 3). The low intensity of the $\pi^*-\pi^*$ band observed for **4** suggests that the $\pi^*-\pi^*$ transition for **2** may be obscured by the tail of the broad IVCT band. We were unable to prepare ($_{NMe2}$I$_2$P$^-$)AlCl$_2$ for comparison to **3**, but **3^{2+}** contains a singly reduced $_{NMe2}$I$_2$P$^-$ ligand and the spectrum indicates that a narrow low-energy band is present as expected for the $\pi^*-\pi^*$ transition. A band at 8052 cm^{-1} ($\varepsilon = 5010$ L mol^{-1} cm^{-1}) observed in the spectrum of a THF solution of **5** was assigned as a metal–ligand charge transfer (MLCT) process (Fig. S8†).[40] The UV-Vis-NIR of **5** has similar transitions to those reported previously by us for the related complex, ($_{dipp}$I$_2$P)AlH(THF).[41]

To more accurately determine ν_{max} and ε_{max} for each of the IVCT bands we fit a series of Gaussian curves under the NIR spectra (Fig. S11–S13†). We first obtained a good fit for the $\pi^*-\pi^*$ transition in the singly reduced ligands and its associated overtones in the spectra of **3^{2+}** and **4**, and this was subtracted from the spectra of **2** and **3** before a fit to the IVCT band was performed. Details of this process are given in the ESI.† In THF solution ν_{max} (ε_{max}) for **1–3** are at 6950 (5110), 7740 (2240), and 7020 (7800) cm^{-1} (L mol^{-1} cm^{-1}), and these values for ε_{max} suggest that **1** and **3** have a delocalized electronic structure whereas **2** is more localized (Table 3). In general, molar absorptivities in excess of 5000 L mol^{-1} cm^{-1}, experimental full width at half maximum, $\Delta\nu_{1/2}$, which is less than the calculated value $\Delta\mathring{\nu}_{1/2}$,[42] and solvent independent values for ν_{max} are the characteristics of delocalized, or Robin and Day Class III compounds. Calculations of $\Delta\nu_{1/2}$ are provided in the ESI (Calculation S5†).

To characterize delocalization in MV **2** and **3**, beyond an interpretation of their ν_{max} and ε_{max} values, we first probed the solvent dependence of their ν_{max}. Observed solvent independence is an indication of delocalization whereas solvent dependence of ν_{max} is an indication of a Class II system because it arises from a dipole moment change accompanying the electron transfer event, or the reorganization energy needed to transfer an electron from one ligand to the other. NIR spectra of **2** were collected in benzene, THF and MeCN which span a dielectric constant range of 34.3, as others have done (Fig. 3).[1,9] Compound **3** was unstable in MeCN solution, and so it was studied in benzene and THF only which have dielectric constant difference of 5.3. Solvent independence, defined as

Table 3 NIR spectroscopy parameters for **1–4** in various solvents and charge states. The parameters were determined from the Gaussian fits to the experimental data (see ESI)

|	Solvent	ν_{max} (cm^{-1})	ε_{max} (M^{-1} cm^{-1})	$\Delta\nu_{1/2}$ (expt) (cm^{-1})	$\Delta\nu_{1/2}$ (calc)^a (cm^{-1})	Γ^c
1	Benzene	6909	6800	2279	3995	0.35
	THF	6950	5110	2410	4007	0.40
	MeCN	6850	4950	2574	3978	0.43
2	Benzene	7590	3300	3840	4190	0.08
	THF	7740	2240	3700	4230	0.12
	MeCN	7720	2000	4220	4220	0
3	Benzene	6900	4350	3230	3990	0.19
	THF	7020	7800	2990	4030	0.26
K$_2$-**1**	THF	8980	3910	6710 (6090)^b	4560	−0.34
(K:18-C-6)$_2$-**1**	THF	6850	5830	5890 (4700)^b	3980	−0.18
K$_2$-**2**	THF	7400	5380	5600 (4854)^b	4130	−0.17
(K:18-C-6)$_2$-**2**	THF	7410	5140	5590 (5003)^b	4137	−0.21
K$_2$-**3**	THF	9780	6350	4470	4753	0.06
(K:18-C-6)$_2$-**3**	THF	9680	6580	4490	4729	0.05
4^d	Benzene	6190	780			
($_{OMe}$I$_2$P$^-$)AlCl$_2$^{d}	THF	6036	2320			

^{a} Calculated from eqn (S7). ^{b} High-energy Gaussian fit gave a large overestimation in $\Delta\nu_{1/2}$ and so the $\Delta\nu_{1/2}$ read directly from the data is given in parentheses (and can be considered the lower limit for $\Delta\nu_{1/2}$). ^{c} Calculated using eqn (S6). ^{d} Absorption bands are not IVCT so parameters $\Delta\nu_{1/2}$ (calc), $\Delta\nu_{1/2}$ (expt), and Γ were not calculated.

$\Delta\nu_{max} < 200$ cm^{-1}, was observed for the IVCT in each of **1–3**, and this suggests a delocalized electronic structure, consistent with the Class III Robin and Day classification, for each compound (Calculations S3, S4 and Tables S5, S6†). As a final probe of delocalization in **1–3** we employed the parameter Γ, which calculates the deviation of the calculated $\Delta\nu_{1/2}$ from the experimental $\Delta\mathring{\nu}_{1/2}$ (Table 3 and Calculation S5†).[38] Based on these combined analyses, **1** and **3** satisfy the criteria for a delocalized description of the MV state. The higher ν_{max}, lower extinction coefficients, large full width at half maximum, and smaller value of Γ for **2** all point to a description of the electronic structure that is localized, or Class II. However, the lack of solvent dependence supports the more intermediate Class II/III designation. Another difference in the NIR spectra of **2** *versus* **1** and **3** is the band shape which is almost symmetric for **2** and characteristic of a Class II system (Fig. 3, S11 and S12†). Bands that are truncated on the low energy side, as observed for **1** and **3**, are distinctive for Class III. Taken together, the experimental data for **2** supports a Class II or II/III designation.

The NIR spectra of THF solutions of K$_2$-**1**–K$_2$-**3** were collected on samples generated by *in situ* reduction of **1–3** using 2.1 equivalents

Scheme 2 Preparation of (K:18-C-6)$_2$-**1**–(K:18-C-6)$_2$-**3**.

of K metal in THF (Scheme 2 and Fig. 3). A shift in the IVCT transitions of 2030 and 2760 cm^{-1} for **1** and **3**, respectively, to higher energy was observed upon reduction. The NIR spectra for K$_2$-**1**, K$_2$-**2** and K$_2$-**3** were also fit to a Gaussian profile to more accurately determine their features (Fig. S14–S16† and Table 3) In each case, the ε_{max} decreases by about 1200 L mol^{-1} cm^{-1}. Based on this data K$_2$-**1** and K$_2$-**3** have Class II characteristics since an increase in optical transition energy is expected when the reorganization energy of a MV system increases.[43] A smaller, 340 cm^{-1} shift to lower energy was observed upon reduction of **2** to K$_2$-**2** along with a 3140 L mol^{-1} cm^{-1} increase in ε_{max}. The parameter Γ is <0 and this suggests K$_2$-**2** should be considered more localized as was observed for **2**. Inspection of the Γ parameter for K$_2$-**3** and for K$_2$-**1** also suggests a localization of the electronic structure relative to **3** and **1**. Electron paramagnetic resonance (EPR) spectra of **2** were collected and those data were consistent with the results of the NIR spectra (see discussion in the ESI and Fig. S17†).

Localization of electrons is known to arise in many cases from the interaction of alkali metal cations with MV compounds,[44,45] and the observed nuances in the absorption spectra can arise from factors such as coulombic effects, precursor formation, changes to the activation barrier for delocalization,[38] and dynamical effects.[46] To assess any potential localization effects associated with the K$^+$ and Na$^+$ cations generated during reduction of **1–3** we probed the spectra of K$_2$-**1**–K$_2$-**3** in the presence of 2 equivalents of the K$^+$ sequestering ligand 18-crown-6 (denoted as 18-C-6). After addition of 18-C-6 to the THF solutions, NIR spectra were collected after solutions had equilibrated for 2 hours. For (K:18-C-6)$_2$-**1**, ε_{max} increased by 1920 L mol^{-1} cm^{-1} and ν_{max} decreased by 2130 cm^{-1}, relative to spectra of K$_2$-**1**. The parameter Γ also increased by 0.16 and these features are consistent with some used to generate K$_2$-**1**–K$_2$-**3** is compatible with THF solution only, not with MeCN or benzene, and so potential solvent delocalization (Fig. 3 and Table 3). For K$_2$-**2** and K$_2$-**3**, only minimal changes in the spectra were
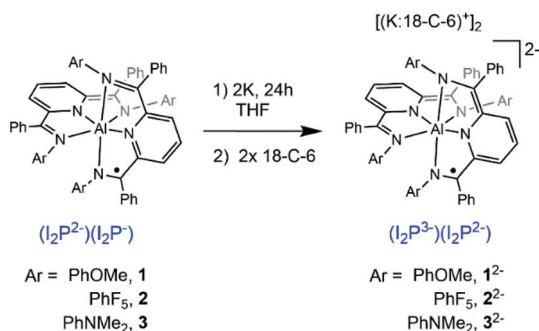
observed upon addition of 18-C-6. The larger spectral shifts observed for K$_2$-**1**, relative to K$_2$-**2** and K$_2$-**3**, in the presence of 18-C-6 are attributed to the ability of the OMe functional groups to sequester the K$^+$ cations, whereas the F- and NMe$_2$-substituted compounds appear to interact less effectively with K$^+$. The chemical reduction process dependence of the IVCT of these compounds was not interrogated.

It is common for counter ions such as alkali metal cations to localize MV compounds and therefore the observations that the spectra of K$_2$-**2** and K$_2$-**3**, are relatively unaffected by sequestration of the K$^+$ ions is unusual. For example, an anionic MV diiron complex was reported where the two redox-active ends are highly charged: [Fe^{II}(CN)$_5$-bridge-Fe^{III}(CN)$_5$]$^{5-}$. Addition of small monoatomic cations such as Na$^+$, Ca^{2+} and La^{3+} to solutions of the diiron complexes resulted in shifts of up to 1690 cm^{-1} in ν_{max}.[45]

Taken together, the information on ν_{max}, ε_{max}, and Γ for (K:18-C-6)$_2$-**1**, (K:18-C-6)$_2$-**2**, and (K:18-C-6)$_2$-**3** suggest that each of these species exhibit some characteristics of localization and some associated with delocalization of the unpaired electron. Intense IVCT bands ($\varepsilon_{max} > 5000$ L mol^{-1} cm^{-1}) with band shapes that are truncated on the lower energy side imply delocalization. Arguing against a delocalized assignment for the electronic states, each of (K:18-C-6)$_2$-**1**, (K:18-C-6)$_2$-**2**, and (K:18-C-6)$_2$-**3** have experimental $\Delta\nu_{1/2}$ greater than the calculated $\Delta\nu_{1/2}$. These combined data lead us to assign each compound as within the Class II/III borderline region. The loss of delocalization in the MV state for **1** and **3** when these compounds are reduced to MV (K:18-C-6)$_2$-**1** and (K:18-C-6)$_2$-**3** is consistent with a potential electrostatic effect arising from higher population of the π^* orbitals following reduction. In contrast (K:18-C-6)$_2$-**2** and **2** have a similar electronic structures bordering Class II/III and **2** is the more localized of those two compounds.

We also probed the possibility that uncharged **1** could interact with added alkali metal cations. Aliquots of NaOTf were added to solutions of **1** in THF and ν_{max} and ε_{max} were monitored with each addition. No change in ν_{max} was observed, but changes in ε_{max} were distinct (Fig. S17† left). Addition of 0.2 equivalents of NaOTf produced a 9% increase in ε_{max} and this was followed by a linear decrease as 1–6 equivalents of the salt were titrated. After accounting for dilution effects, ε_{max} decreased from 9547 for **1** to 6808 M^{-1} cm^{-1} for a solution of **1** containing 6 equivalents of NaOTf (Fig. S17† inset).

Conclusions

In this report we have described a systematic substitution of ED or EW functional groups onto MV complexes that are comprised of redox-active ligand end groups bridged by aluminum. Our previous work with this class of compound assigned delocalized, Class III electronic structures based on experimental observations of the NIR and EPR spectroscopic characterization. In that prior work no understanding of the origin of the delocalization was obtained.

The results of this synthetic study show that electronic coupling between the ligand end groups does not undergo abrupt or unpredictable changes when ED and EW substituents are included in the framework. We propose that this can be attributed to the electronic structure where both metal and ligand have valence p-orbitals and metal and ligand frontier orbitals are well-matched in energy. LMCT and MLCT transitions often localize the electronic structure in transition element MV complexes; whether the metals are end-groups bridged by an organic moiety or the metal bridges two organic fragments. LMCT or MLCT transitions between ligand and Al(III) are not observed and so that mechanism for localization of the electronic structure is not at play here. Instead, the localization effects observed here are more predictably tuned by small degrees. We have also demonstrated in this work that the delocalized MV states are relatively unperturbed by the addition of alkali metal cations, except in the case of **1** where the ligand substituents, –OMe, behave as ligands to chelate the cations.

In summary, a systematic synthetic approach has demonstrated that octahedral Al redox-active ligand MV complexes display delocalization that is tunable similar to organic MV compounds, while the ease of synthesis and access to multiple charge states is more reminiscent of transition element MV compounds. The combination of these two traits promise access to future advances in delocalized materials comprised of main-group elements.

Conflicts of interest

There are no conflicts to declare.

Acknowledgements

Notes and references

1 A. Giraudeau, H. J. Callot and M. Gross, *Inorg. Chem.*, 1979, **18**, 201–206.

2 M. B. Robin and P. Day, *Adv. Inorg. Chem. Radiochem.*, 1968, **10**, 247–422.

3 (*a*) J.-P. Launay, *Eur. J. Inorg. Chem.*, 2020, 329–341; (*b*) M. Parthey and M. Kaupp, *Chem. Soc. Rev.*, 2014, **43**, 5067–5088; (*c*) J. Hankache and O. S. Wenger, *Chem. Rev.*, 2011, **111**, 5138–5178.

4 W. Kaim, A. Klein and M. Glöckle, *Acc. Chem. Res.*, 2000, **33**, 755–776.

5 R. W. Callahan, F. R. Keene, T. J. Meyer and D. J. Salmon, *J. Am. Chem. Soc.*, 1977, **99**, 1064–1073.

6 T. Scheiring, W. Kaim, J. A. Olabe, A. R. Parise and J. Fiedler, *Inorg. Chim. Acta*, 2000, **300**, 125–130.

7 E. T. Seto, R. F. Nelson, J. M. Fritsch, L. S. Marcoux, D. W. Leedy and R. N. Adams, *J. Am. Chem. Soc.*, 1966, **88**, 3498–3503.

8 D. Lorcy, R. Carlier, A. Robert, A. Tallec, P. Le Maguerès and L. Ouahab, *J. Org. Chem.*, 1995, **60**, 2443–2447.

9 H.-J. Yen, H.-Y. Lin and G.-S. Liou, *Chem. Mater.*, 2011, **23**, 1874–1882.

10 G. Chen, I. Mahmud, L. N. Dawe, L. M. Daniels and Y. Zhao, *J. Org. Chem.*, 2011, **76**, 2701–2715.

11 P. Frère, M. Allain, E. H. Elandaloussi, E. Levillain, F.-X. Sauvage, A. Riou and J. Roncali, *Chem.–Eur. J.*, 2002, **8**, 784–792.

12 C. Desmarets, B. Champagne, A. Walcarius, C. Bellouard, R. Omar-Amrani, A. Ahajji, Y. Fort and R. Schneider, *J. Org. Chem.*, 2006, **71**, 1351–1361.

13 M. Yano, Y. Ishida, K. Aoyama, M. Tatsumi, K. Sato, D. Shiomi, A. Ichimura and T. Takui, *Synth. Met.*, 2003, **137**, 1275–1276.

14 (a) C. Lambert, S. Amthor and J. Schelter, *J. Phys. Chem. A*, 2004, **108**, 6474–6486; (b) S. Yamamoto, K. Kuribayashi, T. N. Murakami, E. Kwon, M. J. Stillman, N. Kobayashi, J. Segawa and M. Kimura, *Chem.–Eur. J.*, 2017, **23**, 15446–15454.

15 A. Heckmann and C. Lambert, *Angew. Chem., Int. Ed.*, 2012, **51**, 326–392.

16 G. Valverde-Aguilar, X. Wang, E. Plummer, J. V. Lockard and J. I. Zink, *J. Phys. Chem. A*, 2008, **112**, 7332–7341.

17 Selected examples include: (a) R. M. Buchanan and C. G. Pierpont, *J. Am. Chem. Soc.*, 1980, **102**, 4951–4957; (b) M. L. Kirk, D. A. Shultz, R. D. Schmidt, D. Habel-Rodriguez, H. Lee and J. Lee, *J. Am. Chem. Soc.*, 2009, **131**, 18304–18313; (c) R. M. Buchanan, J. Claflin and C. G. Pierpont, *Inorg. Chem.*, 1983, **22**, 2552–2556; (d) B. W. Stein, D. A. Dickie, S. Nedungadi, D. J. R. Brook, D. A. Schultz and M. L. Kirk, *J. Chem. Phys.*, 2019, **151**, 201103.

18 (a) S. C. Jones, V. Coropceanu, S. Barlow, T. Kinnibrugh, T. Timofeeva, J.-L. Brédas and S. R. Marder, *J. Am. Chem. Soc.*, 2004, **126**, 11782–11783; (b) T. Kojima, F. Ogishima, T. Nishibu, H. Kotani, T. Ishizuka, T. Okajima, S. Nozawa, Y. Shiota, K. Yoshizawa, H. Ohtsu, M. Kawano, T. Shiga and H. Oshio, *Inorg. Chem.*, 2018, **57**, 9683–9695; (c) J. S. Hewage, S. Wanniarachchi, T. J. Morin, B. J. Liddle, M. Banaszynski, S. V. Lindeman, S. Bennett and J. R. Gardinier, *Inorg. Chem.*, 2014, **53**, 10070–10084; (d) C. C. Lu, E. Bill, T. Weyhermuller, E. Bothe and K. Wieghardt, *J. Am. Chem. Soc.*, 2008, **130**, 3181–3197.

19 R. M. Clarke, K. Herasymchuk and T. Storr, *Coord. Chem. Rev.*, 2017, **352**, 67–82.

20 Localized MV state with Co^{III} ion: (a) S. K. Larsen and C. G. Pierpont, *J. Am. Chem. Soc.*, 1988, **110**, 1827–1832; (b) E. P. Ivakhnenko, A. G. Starikov, V. I. Minkin, K. A. Lyssenko, M. Y. Antipin, V. I. Simakov, M. S. Korobov, G. S. Borodkin and P. A. Knyazev, *Inorg. Chem.*, 2011, **50**, 7022–7032, delocalized MV state with Fe^{III} ion: (c) A. Rajput, A. K. Sharma, S. K. Barman, D. Koley, M. Steinert and R. Mukherjee, *Inorg. Chem.*, 2014, **53**, 36–48.

21 K. Ray, T. Petrenko, K. Wieghardt and F. Neese, *Dalton Trans.*, 2007, 1552–1566.

22 Y. Shimazaki, T. D. P. Stack and T. Storr, *Inorg. Chem.*, 2009, **48**, 8383–8392.

23 L. Chiang, K. Herasymchuk, F. Thomas and T. Storr, *Inorg. Chem.*, 2015, **54**, 5970–5980.

24 T. Storr, E. C. Wasinger, R. C. Pratt and T. D. P. Stack, *Angew. Chem., Int. Ed.*, 2007, **46**, 5198–5201.

25 L. Chiang, A. Kochem, O. Jarjayes, T. J. Dunn, H. Vezin, M. Sakaguchi, T. Ogura, M. Orio, Y. Shimazaki, F. Thomas and T. Storr, *Chem.–Eur. J.*, 2012, **18**, 14117–14127.

26 A. Arnold, T. J. Sherbow, R. I. Sayler, R. D. Britt, E. J. Thompson, M. T. Muñoz, J. C. Fettinger and L. A. Berben, *J. Am. Chem. Soc.*, 2019, **141**, 15792–15803.

27 T. W. Myers, N. Kazem, S. Stoll, R. D. Britt, M. Shanmugam and L. A. Berben, *J. Am. Chem. Soc.*, 2011, **133**, 8662–8672.

28 C. C. Scarborough, K. M. Lancaster, S. DeBeer, T. Weyhermüller, S. Sproules and K. Wieghardt, *Inorg. Chem.*, 2012, **51**, 3718–3732.

29 C. M. Araujo, M. D. Doherty, S. J. Konezny, O. R. Luca, A. Usyatinsky, H. Grade, E. Lobkovsky, G. L. Soloveichik, R. H. Crabtree and V. S. Batista, *Dalton Trans.*, 2012, **41**, 3562–3573.

30 Similar shifts in redox events observed with substituted I$_2$P complexes: (a) G. M. Duarte, J. D. Braun, P. K. Giesbrecht and D. E. Herbert, *Dalton Trans.*, 2017, **46**, 16439–16445; (b) J. D. Braun, P. A. Gray, B. K. Sidhu, D. B. Nemez and D. E. Herbert, *Dalton Trans.*, 2020, DOI: 10.1039/d0dt00543f.

31 M. V. Ivanov, S. H. Wadumethrige, D. Wang and R. Rathore, *Chem.–Eur. J.*, 2017, **23**, 8834–8838.

32 C. Creutz and M. H. Chou, *Inorg. Chem.*, 1987, **26**, 2995–3000.

33 J.-M. Savéant, *J. Phys. Chem. B*, 2001, **105**, 8995–9001.

34 D. E. Richardson and H. Taube, *Inorg. Chem.*, 1981, **20**, 1278–1285.

35 A. H. Schroeder and S. Mazur, *J. Am. Chem. Soc.*, 1978, **100**, 7339–7346.

36 J. E. Almlöf, M. W. Feyereisen, T. H. Jozefiak and L. L. Miller, *J. Am. Chem. Soc.*, 1990, **112**, 1206–1214.

37 T. Mani, D. C. Grills, M. D. Newton and J. R. Miller, *J. Am. Chem. Soc.*, 2015, **137**, 10979–10991.

38 B. S. Brunschwig, C. Creutz and N. Sutin, *Chem. Soc. Rev.*, 2002, **31**, 168–184.

39 S. D. Glover and C. P. Kubiak, *J. Am. Chem. Soc.*, 2011, **133**, 8721–8731.

40 (a) T. M. Bass, C. R. Carr, T. J. Sherbow, J. C. Fettinger and L. A. Berben, *Inorg. Chem.*, 2020, **59**, 13517–13523; (b) Z. Chen, W. Wang, C. Zhu, L. Wang, X. Fang and Y. Qiu, *Comput. Theor. Chem.*, 2016, **1090**, 129–133.

41 T. W. Myers and L. A. Berben, *J. Am. Chem. Soc.*, 2013, **135**, 9988–9990.

42 C. Creutz, *Prog. Inorg. Chem.*, 1983, **30**, 1–73.

43 V. Balzani, G. Bergamini, S. Campagna and F. Puntoriero, in *Photochemistry and Photophysics of Coordination Compounds I*, ed. V. Balzani, and S. Campagna, Springer, Berlin, 2007, ch. 1, pp. 1–36.

44 P. Piotrowiak and J. R. Miller, *J. Phys. Chem.*, 1993, **97**, 13052–13060.

45 R. L. Blackbourn, Y. Dong, L. A. Lyon and J. T. Hupp, *Inorg. Chem.*, 1994, **33**, 4446–4452.

46 R. A. Marcus, *J. Phys. Chem. B*, 1998, **102**, 10071–10077.